A&A 466, 119–126 (2007)
DOI: 10.1051/0004-6361:20066995

Astronomy & Astrophysics

Radio observations of the *Chandra* Deep Field South

Exploring the possible link between radio emission and star formation in X-ray selected AGN

E. Rovilos[1,2], A. Georgakakis[3], I. Georgantopoulos[1], J. Afonso[4], A. M. Koekemoer[5], B. Mobasher[5], and C. Goudis[1,2]

[1] Institute for Astronomy and Astrophysics, National Observatory of Athens, I. Metaxa & V. Pavlou Str., Palaia Penteli, 15236 Athens, Greece
e-mail: erovilos@astro.noa.gr
[2] Astronomical Laboratory, Department of Physics, University of Patras, 26500 Rio-Patras, Greece
[3] Astrophysics Group, Imperial College, Prince Consort Rd., London SW7 2AZ, UK
[4] Centro de Astronomia da Universidade de Lisboa, Observatório Astronómico de Lisboa, 1349-018 Lisboa, Portugal
[5] Space Telescope Science Institute, 3700 San Martin Drive, Baltimore, MD 21218, USA

Received 21 December 2006 / Accepted 7 February 2007

ABSTRACT

We explore the nature of the radio emission of X-ray selected AGN by combining deep radio (1.4 GHz; 60 μJy) and X-ray data with multiwavelength (optical, mid-infrared) observations in the Extended Chandra Deep Field South (E-CDFS). The fraction of radio detected X-ray sources increases from 9% in the E-CDFS to 14% in the central region of this field, which has deeper X-ray coverage from the 1 Ms CDFS. We find evidence that the radio emission of up to 60% of the hard X-ray/radio matched AGN is likely associated with star-formation in the host galaxy. Firstly, the mid-IR (24 μm) properties of these sources are consistent with the infrared/radio correlation of starbursts. Secondly, most of them are found in galaxies with blue rest-frame optical colours ($U - V$), suggesting a young stellar population. On the contrary, X-ray/radio matched AGN which are not detected in the mid-infrared have red $U - V$ colours suggesting their radio emission is associated with AGN activity. We also find no evidence for a population of heavily obscured radio-selected AGN that are not detected in X-rays. Finally, we do no confirm previous claims for a correlation between radio emission and X-ray obscuration. Assuming that the radio continuum measures star-formation, this finding is against models where the dust and gas clouds associated with circumnuclear starbursts are spherically blocking our view to the central engine.

Key words. surveys – galaxies: active – X-rays: galaxies – radio continuum: galaxies

1. Introduction

A major recent development in extragalactic astronomy is the discovery that a large fraction of the spheroids in the local Universe contain a super-massive black hole (e.g. Magorrian et al. 1998) and that the mass of this monster is tightly correlated to the stellar mass of host galaxy bulge (e.g. Ferrarese & Merritt 2000; Gebhardt et al. 2000). The implication of this fundamental observation is that the formation and evolution of galaxies and the build-up of super-massive BHs at their centers are interconnected. The evidence above has prompted attempts to model the interplay between black-hole growth and star-formation (e.g. Fabian et al. 1998). A recent development in this direction are simulations which include AGN feedback mechanisms (e.g. Hopkins et al. 2005). In these, galaxy mergers trigger the AGN and also produce nuclear starbursts that both feed and obscure the central engine for most of its active lifetime ($\approx 10^8$ yr). AGN-driven outflows also develop, which at later stages become strong enough to rapidly quench the star-formation, leaving behind a red passive remnant and allowing the AGN to shine unobscured for a short period ($\approx 10^7$ yr). The attractiveness of this class of models is that they reproduce a number of AGN properties (e.g. duty-cycle, $N_{\rm H}$ distribution, luminosity function), while they can potentially explain galaxy properties, such as the bimodality of the colour magnitude diagram (e.g. Bell et al. 2004; Willmer et al. 2006; Nandra et al. 2007), via the AGN-driven regulation of the star-formation.

The predictions of the AGN feedback model above include a link between the obscured AGN stage and starburst events. In the local Universe ($z < 0.1$) an association between *optically* selected AGN and recent/ongoing star-formation has been established using the Sloan Digital Sky Survey (SDSS; Kauffmann et al. 2003). The link between obscured accreting BHs and star-formation remains controversial however, despite claims that Seyfert-IIs show optical spectroscopic evidence for young stellar populations (e.g. Cid Fernandes et al. 2001). The low-z results above, although broadly consistent with the merger formation models of Hopkins et al. (2005), are based on optically selected AGN samples, which may miss a substantial fraction of the BH accretion in the Universe (e.g. Mushotzky 2004). At higher redshift in particular ($z \approx 1$), close to peak of the global AGN density (e.g. Barger et al. 2005; Hasinger et al. 2005), X-ray observations are arguably the most efficient tool for identifying AGN over a wide range of luminosities and obscurations. The stellar population of the X-ray selected AGN in deep surveys is still under debate. Franceschini et al. (2005) find that about 40% of the X-ray sources in the ELAIS-N1 SWIRE region have mid-IR SEDs consistent with ongoing star-formation. Contamination of these wavelengths from hot dust emission related to the central accreting BH remains an issue however, when

interpreting the mid-IR properties of X-ray sources. Recently, Nandra et al. (2007) find that the majority of the $z \approx 1$ X-ray sources in the AEGIS survey (Davis et al. 2007) have rest-frame colours of passive red galaxies indicating a dominant old stellar population with little, if any, current star-formation.

One of the difficulties in studying the stellar content of AGN hosts is the decomposition of the stellar light from the emission of the accreting BH. Combining information from different parts of the electromagnetic spectrum is essential to address this issue. In this paper we follow such a multiwavelength approach to study the nature of the μJy radio emission of X-ray sources in the Extended Chandra Deep Field South (E-CDFS) and to explore the implications in the context of the AGN/star-formation connection. This is motivated by previous claims that X-ray selected type-II (X-ray absorbed) AGN are more frequently associated with μJy flux density radio sources (Bauer et al. 2002; Georgakakis et al. 2004). At these faint limits the radio population is dominated by starbursts (Georgakakis et al. 1999; Chapman et al. 2003; Afonso et al. 2005) and therefore, the above finding has been tentatively interpreted as evidence for a link between star-formation and obscured AGN. The radio luminosities of these systems ($\approx 10^{23}$ W Hz^{-1}) are well below those of the classic radio galaxies ($>10^{24}$ W Hz^{-1}), suggesting that star-formation may contribute or even dominate the observed radio emission.

In addition to the deep X-ray observations in the E-CDFS the multiwavelnegth data used here include ultra-deep wide-area radio 1.4 GHz observations (60 μJy; 0.3 deg^2; Afonso et al. 2006), Spitzer mid-IR photometry as part of the Great Observatories Origins Deep Survey (GOODS) as well as extensive optical photometric and spectroscopic follow-up programs. These complementary multiwavelength observations are essential to explore the nature of the μJy radio emission in X-ray selected AGN. Throughout this paper we adopt $H_0 = 72$ km s^{-1} Mpc^{-1}, $\Omega_{\rm M} = 0.3$ and $\Omega_\Lambda = 0.7$.

2. The data

The X-ray observations are from the 1 Ms CDFS and the E-CDFS. These two surveys cover a total contiguous area of 0.3 deg^2 to a limiting 2–8 keV flux of $\approx 2.8 \times 10^{-16}$ erg cm^{-2} s^{-1} at the most sensitive central region of the CDFS increasing to $\approx 6.7 \times 10^{-16}$ erg cm^{-2} s^{-1} in the E-CDFS. In this paper we use the X-ray point source catalogs constructed by Alexander et al. (2003) and Lehmer et al. (2005) for the CDFS and E-CDFS respectively.

The radio data are presented in Afonso et al. (2006) and more analytically in Koekemoer et al. (in preparation). In brief, the observations are performed at 1.4 GHz using the Australia Telescope Compact Array (ATCA) and cover a total area of 1.2 deg^2 that includes both the CDFS and the E-CDFS (see Fig. 1). 120 h of data were obtained, causing the 1σ rms noise level to range from 14 μJy at the central part to 100 μJy at the outer region, while the beam size used for imaging is (16.8×6.95) arcsec. Its shape is a result of the ATCA configuration, which is more spread in the E-W direction, and this reflects also to the positional uncertainties, which are larger in declination. The sources are selected using the False Discovery Rate method. The final list comprises 681 sources with integrated flux densities ranging from 61 μJy to 170 mJy. A total of 133 and 337 sources overlap with the CDFS and the E-CDFS respectively.

Mid-infrared MIPS-24 μm data are available as part of the Great Observatories Origins Deep Survey (GOODS) Legacy Survey. The observations were carried out by the Spitzer Space Telescope and cover a total area of about 10×16.5 arcmin^2 centered on the CDFS (see Fig. 1). We have used the public catalog[1], which contains 948 sources to the limit of 80 μJy.

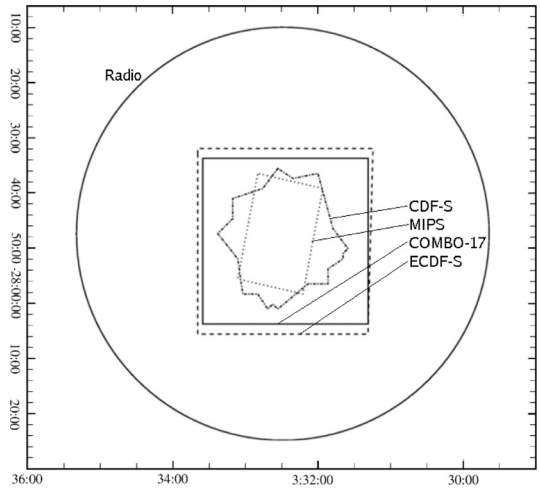

Fig. 1. Layout of the multiwavlength observations in the E-CDFS. The dot-dashed and dashed lines delineate the 1 Ms CDFS and the shallower 250 ks E-CDFS respectively. The circle marks the limits of the ATCA radio observations. The continuous-lined square marks the boundaries of the COMBO-17 survey and the the dotted line the area covered by the Spitzer/MIPS observations.

Multi-waveband optical/near-IR photometric as well as optical spectroscopic observations have been carried out by many groups in the CDFS and E-CDFS survey regions, providing redshift estimates (spectroscopic or photometric) for different source populations. The spectroscopic redshifts used here are from Szokoly et al. (2004), Vanzella et al. (2005, 2006), Le Fèvre et al. (2004) and Mignoli et al. (2005). For sources without spectroscopic redshifts we rely on photometric redshifts mainly from Wolf et al. (2004) as part of the COMBO-17 survey. This uses 17 photometric passband and three sets of template SED (stars, galaxies and QSOs) to determine the redshifts of ~65 000 objects with an accuracy of a few percent (up to 10% for $R \gtrsim 24$). The area covered by COMBO-17 covers the CDFS and most of the E-CDFS (see Fig. 1). Photometric redshifts from Zheng et al. (2004) are also used in the case of CDFS X-ray sources fainter than the COMBO-17 magnitude limit.

3. The sample

Given the positional uncertainties of the X-ray and radio sources we search for counterparts in a radius corresponding to the 3σ radio positional uncertainty. For most cases the radio/X-ray offset is less than 3 arcsec. We find 44 and 72 matches for the CDFS and the E-CDFS respectively with 27 common identifications. We quantify the fraction of spurious matches using mock catalogs produced by randomly shifting the positions of X-ray and radio sources adopting a maximum offset of 0.5 arcmin. The fraction of spurious identifications is estimated to be 1.8% and 2.4% of the X-ray/radio matched population for the CDFS and E-CDFS respectively. Searching for mid-infrared counterparts for CDFS sources using a 3 arcsec search radius returned 133 matches, 32 of which have radio counterparts. Searching for matches among the radio sources which are inside the CDFS (133 sources) returned 52 matches.

[1] http://data.spitzer.caltech.edu/popular/goods/.

The radio detection rates for the CDFS and E-CDFS X-ray sources are thus 14% and 9% respectively, while the X-ray detection rates for radio sources are 33% for the CDFS and 21% for the E-CDFS case. The radio and X-ray detection rates measured in Bauer et al. (2002) are 26% and 71% respectively for the 1 Ms *Chandra* Deep Field North (CDF-N). The 1 Ms CDF-N X-ray catalog has a flux limit of $\approx 1 \times 10^{-16}$ erg cm^{-2} s^{-1}, marginally fainter than the CDFS (1.3×10^{-16} erg cm^{-2} s^{-1} in the full band). The radio flux density limit in Bauer et al. (2002) is ≈ 40 μJy, while our detection threshold in the central region is ≈ 60 μJy. It is interesting to note that both the X-ray and radio detection rates increase with deeper observations. Bauer et al. (2002) report that a large fraction of their radio-X-ray matched sources lie close to their detection limit, so deeper radio observations would increase the detection rate.

Table 1 lists the basic X-ray, radio and infrared properties of the 89 unique matches. the columns are:

1. Identification number in the Alexander et al. (2003) catalog.
2. Identification number in the Lehmer et al. (2005) catalog.
3. X-ray position Right Ascension (J2000).
4. X-ray position Declination (J2000).
5. Spectroscopic (if available) or photometric redshift.
6. Hard band (2.0−8.0 keV) X-ray flux. The fluxes have been calculated from the hard-band count rates assuming a power-law spectrum with an intrinsic photon index $\Gamma = 1.9$ (Nandra & Pounds 1994) and are corrected for absorption.
7. Hard band X-ray rest-frame luminosity based on the above fluxes and corrected for intrinsic absorption.
8. Hardness ratio, $HR = \frac{H-S}{H+S}$, where H and S are the count rates in the hard (2−8 keV) and soft (0.5−2 keV) bands respectively.
9. Hydrogen column density calculated using the hardness ratio of each source and assuming an intrinsic power-law X-ray spectrum with $\Gamma = 1.9$ and a Galactic column density of $N_{\rm H} = 10^{20}$ cm^{-2} appropriate for the CDFS.
10. Radio (rest-frame) luminosity, assuming a radio spectral index of 0.8 ($f_{1.4\ \rm GHz} \propto \nu^{-\alpha}$). This may overestimate the radio luminosity of AGN dominated systems, as their radio spectrum is flatter because of synchrotron self absorption (e.g. Taylor et al. 1996).
11. 24 μm rest frame luminosity. We have used the SED of NGC 1068 (Lutz et al. 1997), a typical Seyfert-2, to perform the K-correction. Using starburst galaxy SEDs, such as M 82 or Arp 220, would result in larger K-corrections at $z \approx 1.4$, because of the strong absorption from PAHs and silicate features at $\lambda \approx 10$ μm.
12. Source classification based on the X-ray luminosity (not corrected for absorption) and the hardness ratio according to scheme:
    - Galaxies, if $L_{\rm x} < 10^{42}$ erg s^{-1} and $HR \leq -0.2$,
    - AGN2, if $HR > -0.2$,
    - AGN1, if $L_{\rm x} \geq 10^{42}$ erg s^{-1} and $HR \leq -0.2$.

    These criteria are similar to those adopted by Bauer et al. (2004). The classification of individual sources presented here is consistent with that study. Sources in the normal galaxy group will not be discussed in the rest of the paper.

4. Results

4.1. The stellar population of AGN

Figure 2 plots the 24 μm MIR luminosity against 1.4 GHz radio power. For starburst galaxies these two quantities are correlated (Appleton et al. 2004; Wu et al. 2005), as both wavelengths are believed to probe the same population of young massive stars. In this figure, many X-ray/radio matched AGN (up to 60% of the hard X-ray/radio population within the MIPS area) scatter around the MIR/1.4 GHz relation of star-forming galaxies (Wu et al. 2005), suggesting ongoing star-formation is likely to dominate the observed radio emission. Moreover, X-ray sources not detected to the limit of the radio survey have $L_{1.4\ \rm GHz}$ upper limits which are also broadly consistent with that relation. This is tentative evidence that a substantial fraction of the overall X-ray selected AGN population have MIR and radio properties consistent with star-formation in the host galaxy. The radio observations are not deep enough to detect these systems, although Spitzer/MIPS is sufficiently sensitive to identify this population at 24 μm. In Fig. 2 there are also X-ray/radio matched AGN that deviate from the MIR/1.4 GHz relation of star-forming galaxies. These include sources without 24 μm counterparts, plotted as upper limits and radio loud AGN, defined as sources with $\log L_{1.4\ \rm GHz} > 10^{25}$ W Hz^{-1} (Kellermann et al. 1989). The radio emission of both these populations is associated with accretion on a supper-massive BH.

Donley et al. (2005) report a population of radio selected AGN not detected in X-rays but identified by their excess radio to infrared emission. Figure 2 plots the infrared/radio sources not identified with the 1 Ms exposure of the CDFS with open circles. There is no significant deviation of those sources from the correlation line, suggesting they, too, are of starburst nature. We therefore cannot confirm the result of Donley et al. (2005) based on radio sources detected by MIPS. There are however radio sources without neither an X-ray nor a MIPS detection which can be considered being of radio excess based on their infrared upper limits. See also recent results from Barger et al. (2007).

A complementary approach for studying the stellar population of AGN hosts is to use the colour-magnitude diagram (CMD), which provides a powerful diagnostic for separating evolved from star-forming galaxies (e.g. Bell et al. 2004; Willmer et al. 2006; Nandra et al. 2007). Figure 3 shows the CMD for the hard X-ray selected AGN in comparison with optically selected galaxies from the COMBO-17 in the redshift interval $0.2 < z < 1.2$. For clarity radio loud AGN are not plotted. X-ray sources in this figure are preferentially associated with relatively luminous galaxies evenly spread between the blue and the red clouds. This suggests a mix of early and late-type hosts.

X-ray/radio matched AGN that scatter around the MIR/1.4 GHz relation of star-forming galaxies are all found in the blue cloud of Fig. 3. This is further evidence for a young stellar population in these systems that is also likely to dominate the radio luminosity. On the contrary, X-ray/radio matched AGN without MIR counterparts lie in the red cloud, suggesting old stellar populations and radio emission associated with accretion on the central BH. These same sources also deviate from the MIR/1.4 GHz relation of star-forming galaxies, consistent with their position in the CMD.

We caution for two effects that may bias the position of AGN in the colour–magnitude. The red colour of some AGN may partly be a result of dust extinction, while scattered/direct light from the AGN itself may shift the rest-frame colours of some sources toward the blue cloud. Visual inspection of HST/ACS images suggests that for some systems this is indeed the case. Nevertheless, for most X-ray sources in the sample the optical colours are dominated by the host galaxy with small contamination from the central engine. A thorough analysis of these effects will be presented in a future publication (Rovilos et al., in preparation).

Table 1. X-ray, radio and infrared properties of all X-ray sources matched with radio counterparts.

A03	L05	α (J2000)	δ (J2000)	z	f_x (2−8) keV ($\times10^{-16}$ erg cm^{-2} s^{-1})	log L_x (2−8) keV (erg s^{-1})	HR	log N_H (cm^{-2})	log $L_{1.4\ GHz}$ (W Hz^{-1})	log $L_{24\ \mu m}$ (W Hz^{-1})	Type
12	–	3:31:51.16	−27:50:51.6	0.674	9.75	42.24	−0.29	21.96	23.09	–	AGN1
27	240	3:31:57.71	−27:42:08.4	0.654[1]	28.94	42.68	−0.34	21.76	23.37	–	AGN1
37	258	3:32:01.42	−27:46:47.1	1.010[1]	95.81	43.66	0.50	23.15	26.41	23.92	AGN2
48	280	3:32:04.89	−27:41:27.6	0.720	33.94	42.85	>0.51	22.97	23.30	23.27	AGN2
57	–	3:32:07.18	−27:51:28.1	0.350[2]	<3.41	<41.11	<−0.12	22.07	22.70	–	Galaxy
65	–	3:32:08.50	−27:46:48.6	0.310	7.17	41.32	>0.29	22.48	22.76	23.46	AGN2
66	305	3:32:08.66	−27:47:34.4	0.543	525.32	43.75	−0.50	20.00	24.32	24.58	AGN1
69	313	3:32:09.69	−27:42:48.4	0.733	<4.82	<42.02	<−0.52	20.00	23.70	–	AGN1
74	–	3:32:10.80	−27:46:27.6	1.013[1]	<2.97	<42.15	<−0.05	22.61	24.34	23.91	AGN1
76	316	3:32:10.91	−27:44:15.1	1.615	75.51	44.05	−0.49	20.00	25.63	24.87	AGN1
78	318	3:32:11.00	−27:40:53.7	0.181	29.31	41.42	−0.40	21.07	22.43	–	Galaxy
88	328	3:32:13.24	−27:42:40.9	0.605	122.69	43.23	0.09	22.52	23.24	24.03	AGN2
109	345	3:32:16.21	−27:39:30.4	1.324	141.21	44.11	−0.52	20.00	24.37	25.21	AGN1
117	348	3:32:17.14	−27:43:03.3	0.569	50.11	42.78	−0.52	20.00	22.98	24.28	AGN1
118	347	3:32:17.18	−27:52:20.9	1.097	117.82	43.84	0.63	23.31	23.56	24.36	AGN2
121	–	3:32:18.07	−27:47:18.2	0.734	<2.62	<41.76	<−0.58	20.00	23.95	–	Galaxy
129	–	3:32:19.81	−27:41:23.1	0.229	<6.50	<40.98	<−0.15	21.91	22.53	23.67	Galaxy
144	–	3:32:22.51	−27:48:04.8	0.167[1]	<2.22	<40.22	<−0.44	20.74	22.05	–	Galaxy
148	–	3:32:22.63	−27:44:26.0	0.737	<3.47	<41.89	0.12	22.64	23.33	24.15	AGN2
153	–	3:32:23.88	−27:58:42.4	0.123[1]	<16.94	<40.81	−0.01	22.00	21.84	–	AGN2
164	–	3:32:25.17	−27:54:49.6	1.090	22.45	43.11	>0.69	23.35	23.64	23.94	AGN2
177	379	3:32:27.00	−27:41:05.1	0.734	539.43	44.07	−0.53	20.00	25.64	24.38	AGN1
181	–	3:32:28.73	−27:46:20.2	0.738	1.69	41.58	−0.67	20.00	23.72	–	AGN1[3]
189	390	3:32:29.88	−27:44:25.0	0.076	<3.15	<39.62	<−0.79	20.00	22.18	23.01	Galaxy
193	–	3:32:30.06	−27:45:23.5	0.960	17.46	42.87	−0.57	20.00	23.68	24.34	AGN1
192	392	3:32:30.01	−27:44:04.0	0.076	5.65	39.88	−0.56	20.00	21.80	22.80	Galaxy
197	–	3:32:31.47	−27:46:23.0	2.223	<2.57	<42.91	<0.02	23.24	24.27	25.27	AGN1
219	–	3:32:35.72	−27:49:16.0	2.578	4.40	43.30	0.30	23.64	24.48	25.67	AGN2
228	–	3:32:37.20	−27:57:47.5	0.132[1]	<9.95	<40.65	<0.24	22.26	21.77	–	Galaxy
230	414	3:32:37.77	−27:52:12.4	1.603	68.48	44.00	−0.51	20.00	24.10	25.43	AGN1
240	420	3:32:38.92	−27:57:00.4	0.304[1]	230.43	42.81	0.44	22.59	22.49	23.99	AGN2
245	425	3:32:39.68	−27:48:50.7	3.064	45.34	44.48	0.18	23.67	24.61	25.31	AGN2
247	433	3:32:40.84	−27:55:46.6	0.625	57.44	42.93	0.40	22.82	23.18	24.05	AGN2
260	445	3:32:44.28	−27:51:41.0	0.279	<2.86	<40.82	<−0.71	20.00	23.07	24.20	Galaxy
265	–	3:32:44.98	−27:54:38.7	0.458	<4.57	<41.52	<−0.09	22.19	22.94	23.82	Galaxy
270	460	3:32:46.76	−27:42:12.6	0.103	<7.04	<40.27	<−0.63	20.00	21.53	22.17	Galaxy
274	464	3:32:47.86	−27:42:32.8	0.979	206.58	43.96	−0.20	22.36	23.79	24.78	AGN1
278	469	3:32:49.23	−27:40:49.8	1.222	50.15	43.58	>0.49	23.25	25.60	25.44	AGN2
284	–	3:32:51.78	−27:44:35.7	0.522	<4.40	<41.64	<−0.09	22.24	23.02	24.11	Galaxy
285	488	3:32:51.83	−27:42:28.9	1.027	<11.28	<42.75	<−0.11	22.54	23.90	24.61	AGN1
302	518	3:32:59.31	−27:48:58.5	1.280[2]	59.02	43.70	0.52	23.31	23.74	25.03	AGN2
315	544	3:33:02.97	−27:51:46.4	3.690[2]	7.32	43.88	−0.55	20.00	24.87	25.63	AGN1
325	592	3:33:09.48	−27:46:03.4	0.347	39.06	42.17	−0.19	21.94	22.65	–	AGN2
326	597	3:33:10.18	−27:48:41.8	0.812[1]	89.84	43.40	−0.40	21.54	25.78	–	AGN1
–	7	3:31:15.04	−27:55:18.6	0.494[1]	284.67	43.39	−0.40	21.33	24.15	–	AGN1
–	46	3:31:24.90	−27:52:07.9	1.262[1]	45.16	43.57	−0.47	20.00	26.51	–	AGN1
–	47	3:31:25.29	−27:59:58.7	0.789[1]	255.87	43.83	0.36	22.90	23.73	–	AGN2
–	51	3:31:27.23	−27:42:46.9	–	15.59	–	−0.18	–	–	–	–
–	66	3:31:30.07	−27:56:02.3	0.690[1]	<7.34	<42.14	<−0.27	22.04	24.34	–	AGN1
–	74	3:31:31.63	−27:45:19.2	0.138[1]	<9.99	<40.69	<−0.13	21.85	20.91	–	Galaxy
–	82	3:31:32.82	−28:01:16.1	0.148[1]	<9.77	<40.75	<−0.13	21.86	22.04	–	Galaxy
–	94	3:31:35.43	−28:03:15.7	0.083[1]	42.74	40.84	−0.64	20.00	21.48	–	Galaxy
–	136	3:31:43.21	−27:54:05.3	–	95.28	–	0.34	–	–	–	–
–	141	3:31:43.48	−27:51:03.0	0.265[1]	<11.79	<41.38	<0.10	22.25	22.26	–	Galaxy
–	146	3:31:44.04	−27:38:35.7	0.057[1]	10.37	39.89	0.41	22.33	21.29	–	AGN2
–	177	3:31:48.57	−28:04:32.9	–	<9.05	–	−0.10	–	–	–	–
–	205	3:31:52.16	−27:39:26.0	–	<7.59	–	<0.05	–	–	–	–
–	254	3:32:00.83	−27:35:56.6	0.948[1]	41.64	43.23	−0.36	21.89	24.90	–	AGN1
–	268	3:32:03.04	−27:35:16.5	0.000	0.00	0.03	−0.03	–	–	–	Star[4]
–	282	3:32:05.21	−28:04:14.7	–	69.15	–	0.02	–	–	–	–
–	289	3:32:06.09	−27:32:36.1	–	142.70	–	−0.22	–	–	–	–
–	321	3:32:11.64	−27:37:26.0	1.574[1]	521.28	44.86	−0.30	22.41	25.75	–	AGN1

Table 1. continued.

A03	L05	α (J2000)	δ (J2000)	z	f_x (2−8) keV ($\times 10^{-16}$ erg cm^{-2} s^{-1})	log L_x (2−8) keV (erg s^{-1})	HR	log N_H (cm^{-2})	log $L_{1.4\ GHz}$ (W Hz^{-1})	log $L_{24\ \mu m}$ (W Hz^{-1})	Type
–	385	3:32:28.56	−27:35:37.0	0.677[1]	717.60	44.12	−0.37	21.65	23.25	–	AGN1
–	398	3:32:32.01	−28:03:09.7	1.966[1]	261.23	44.79	−0.37	22.29	26.79	–	AGN1
–	504	3:32:56.49	−27:58:48.2	0.154[1]	5.74	40.55	−0.33	21.41	22.93	–	Galaxy
–	506	3:32:57.00	−27:33:43.7	–	50.59	–	0.33	–	–	–	–
–	520	3:32:59.54	−28:01:23.7	2.386[1]	26.19	43.99	−0.36	22.52	24.87	–	AGN1
–	538	3:33:01.46	−28:02:51.4	1.265[1]	115.23	43.98	0.11	22.94	24.11	–	AGN2
–	552	3:33:03.76	−27:36:11.0	1.574[1]	25.85	43.56	−0.32	22.37	24.69	–	AGN1
–	555	3:33:04.43	−27:38:01.5	0.991[1]	<9.66	<42.64	−0.09	22.55	23.68	–	AGN2
–	557	3:33:05.13	−27:40:27.6	0.302[1]	<3.68	<41.01	<−0.19	21.90	22.46	–	Galaxy
–	581	3:33:08.16	−27:50:33.2	0.730[1]	34.32	42.87	>0.51	22.98	24.43	–	AGN2
–	587	3:33:09.10	−27:58:46.2	0.674[1]	<7.37	<42.12	<0.21	22.68	23.04	–	AGN1
–	599	3:33:10.28	−27:33:06.5	–	16.09	–	>0.24	–	–	–	–
–	609	3:33:11.77	−27:41:38.6	1.059[1]	5.82	42.49	>−0.15	22.50	24.17	–	AGN2
–	632	3:33:16.14	−28:02:21.0	0.362[1]	16.76	41.85	>0.08	22.32	22.89	–	AGN2
–	639	3:33:16.91	−27:41:21.8	0.143[1]	<17.99	<40.98	<−0.15	21.83	22.16	–	Galaxy
–	646	3:33:17.74	−27:59:06.2	1.128[1]	<11.24	<42.85	<0.25	23.00	24.00	–	AGN1
–	657	3:33:19.09	−27:35:30.9	0.139[1]	<9.04	<40.65	<−0.24	21.65	22.00	–	Galaxy
–	664	3:33:20.55	−27:49:10.9	0.139[1]	<13.86	<40.83	<−0.69	20.00	21.93	–	Galaxy
–	674	3:33:21.29	−27:41:38.6	1.151[1]	<13.69	<42.95	<−0.03	22.71	24.40	–	AGN1
–	676	3:33:22.75	−27:54:59.1	0.831[1]	20.68	42.79	0.37	22.92	23.38	–	AGN2
–	738	3:33:34.56	−27:47:51.0	0.635[1]	99.40	43.19	0.51	22.91	23.93	–	AGN2
–	743	3:33:36.39	−27:43:55.1	1.114[1]	<17.75	<43.03	0.06	22.80	24.30	–	AGN2
–	746	3:33:36.65	−27:42:23.6	–	15.02	–	>0.21	–	–	–	–
–	752	3:33:38.48	−28:02:53.9	–	<20.86	–	<−0.32	–	–	–	–
–	118	3:31:39.99	−27:41:57.2	–	221.99	–	−0.02	–	–	–	–
–	124	3:31:40.99	−27:44:35.0	–	60.28	–	0.06	–	–	–	–
–	606	3:33:11.32	−27:43:11.9	1.051[1]	21.81	43.06	>0.64	23.29	23.76	–	AGN2

Notes:
[1] Photometric redshift from Wolf et al. (2004). [2] Photometric redshift from Zheng et al. (2004). [3] Classified as "galaxy" in Bauer et al. (2004). [4] Galactic star, identified by optical photometry and spectroscopy (Zheng et al. 2004; Szokoly et al. 2004).

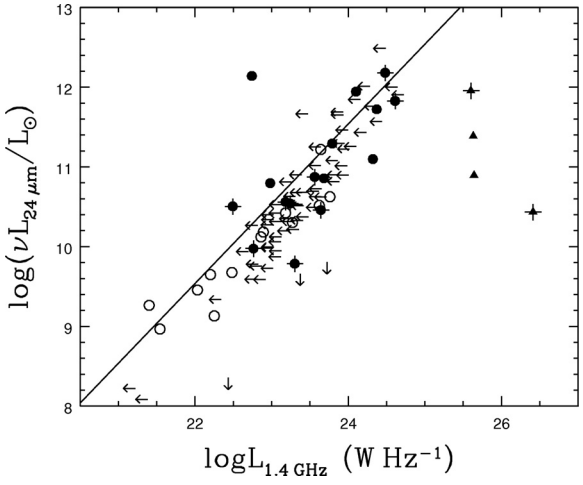

Fig. 2. 24 μm versus radio luminosity. AGN are shown as filled circles and radio loud AGN (with log $L_{1.4\ GHz} > 10^{25}$ W Hz^{-1}) as filled triangles. Crosses mark obscured objects (AGN2). The line is the best fit $L_{24\ \mu m} - L_{1.4\ GHz}$ for Spitzer starburst galaxies (Wu et al. 2005). Open circles represent radio/infrared sources without an X-ray counterpart.

4.2. Radio detection and X-ray obscuration

In this section we explore a possible connection between radio detection and X-ray obscuration suggested in previous studies (e.g. Bauer et al. 2002; Georgakakis et al. 2004). Figure 4 plots the hardness ratio against the intrinsic hard X-ray luminosity. AGN with radio counterparts are plotted with filled circles, while AGN not detected in the radio are shown as crosses. For clarity, X-ray sources without radio identifications are from the CDFS only. Filled triangles mark radio loud sources.

In Fig. 4 there is no obvious tendency of radio detected sources to be harder, in other words more obscured. This is further demonstrated in Figs. 5 and 6, plotting the HR and N_H distributions respectively of X-ray sources with and without radio identifications. We quantify the differences between these two populations using the Gehan's statistical test as implemented in the ASURV package (Isobe et al. 1986; Lavalley et al. 1992) to take into account HR/N_H lower limits. This exercise does not show any statistically significant differences in the obscuration properties of X-ray sources with and without radio matches. The probability that these two populations are drawn from the same parent distribution is >18% for all the panels in Figs. 5 and 6.

5. Discussion

5.1. AGN – Starburst connection

In the local Universe there is strong observational evidence, embodied in the $M_{BH} - \sigma$ relation (e.g. Ferrarese & Merritt 2000; Gebhardt et al. 2000), that the the build-up of the stellar mass of galaxies and the growth of the super-massive BH at their centers are intimately related. At higher redshift, $z \approx 1$, close to the peak of the AGN density in the Universe (e.g. Barger et al. 2005), clear-cut examples of accreting BHs associated with starburst events remain to be identified. The sensitivity of *Spitzer* in the

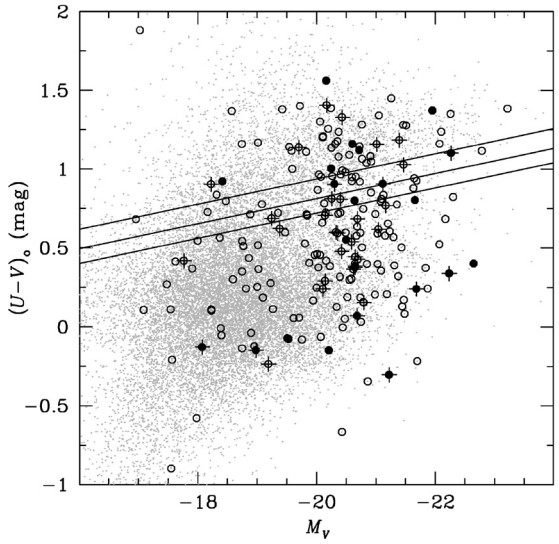

Fig. 3. Colour–magnitude diagram for hard X-ray selected AGN in the redshift interval $0.2 < z < 1.2$ probed by the COMBO-17 survey. Open circles are X-ray sources without radio counterparts while filled circles correspond to X-ray/radio matches. X-ray sources detected at 24 μm are marked with a cross. Optically selected galaxies in the same redshift range from the COMBO-17 photometric survey are plotted as gray dots. The lines mark the borders of the red cloud for redshifts 0.5, 0.9 and 1.2, according to the relation $\langle U-V\rangle = 1.15-0.31z-0.08(M_V-5\log h+20)$ with $h = 0.72$ (Bell et al. 2004).

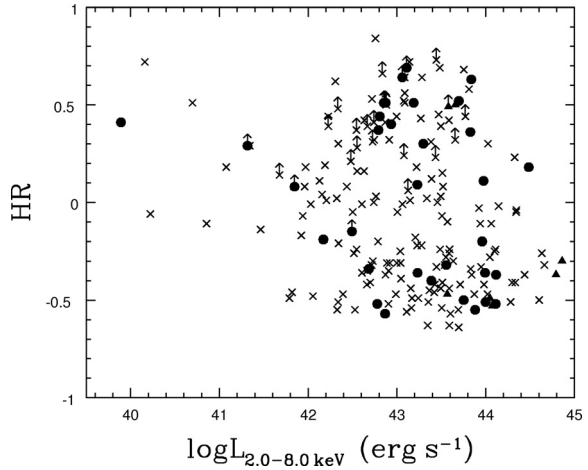

Fig. 4. Hardness ratio against hard band X-ray luminosity. Filled circles are X-ray/radio matches from both the CDFS and the E-CDFS. Filled triangles are radio loud AGN $\left(\log L_{1.4\ \mathrm{GHz}} > 10^{25}\ \mathrm{W\ Hz^{-1}}\right)$. Non-radio detected X-ray sources (CDFS only for clarity) are plotted with a cross.

mid-infrared has motivated studies that use these wavelengths to explore the stellar population of AGN hosts (e.g. Franceschini et al. 2005). The main issue with any such observational program however, relates to the difficulty in deconvolving the AGN from the star formation emission. In this paper we follow a multi-wavelength approach to explore the extent to which the faint radio emission measures the level of star formation at $z \approx 1$.

We have seen that a fraction (14% and 11% for the CDFS and E-CDFS respectively) of the hard X-ray selected AGN have a radio counterpart. Radio emission can be generated in a starburst (e.g. Condon et al. 1991), but it is also known to emerge from powerful quasars in the form of radio jets and lobes (Fanaroff & Riley 1974). Also low luminosity AGN produce radio power as

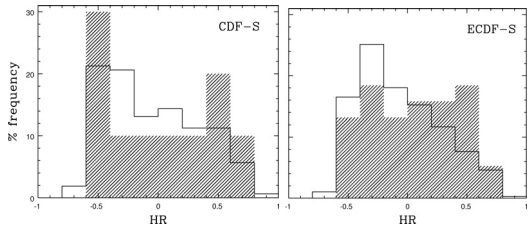

Fig. 5. Hardness ratio distribution of X-ray sources with radio detections (shaded) and without radio counterparts. The *left panel* is for the CDFS and the *right panel* is for the E-CDFS.

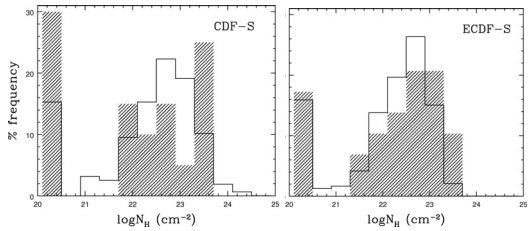

Fig. 6. Hydrogen column density N_H histogram for radio detected (shaded) and not detected X-ray sources for the CDFS (*left*) and the E-CDFS (*right*).

a result of their nuclear activity (Falcke et al. 2000; Nagar et al. 2002). We use the radio-infrared correlation to discriminate between the two possible mechanisms generating radio emission, since there is a close correlation between infrared and starburst generated radio (Helou et al. 1985; Bressan et al. 2002). In cases of a starburst/AGN co-existence, Farrah et al. (2003) using SED fitting to Ultra Luminous Infrared Galaxies, have shown that such a correlation is attributed to the starburst part of the emission, while the infrared is not correlated with the AGN generated radio. Therefore, the bulk of the radio emission from a large fraction (up to 60%) of our sample is likely to be starburst powered. In addition to that, a large fraction of the X-ray population not detected at 1.4 GHz lies in the blue cloud of the color–magnitude diagram and has radio luminosity upper limits that are consistent with the $L_{24\ \mu\mathrm{m}} - L_{1.4\ \mathrm{GHz}}$ relation for starbursts. It is therefore possible that a large fraction of the X-ray selected AGN at $z \approx 1$ are associated with star-formation

The detection of star formation in X-ray selected AGN is an important result and adds to the lines of evidence that there is a starburst-AGN relation. These phenomena are often found in the same systems in cases of ultra-luminous infrared galaxies (see Sanders & Mirabel 1996) and also in other, optically and X-ray selected galaxies (e.g. Kauffmann et al. 2003; Franceschini et al. 2005). While both phenomena have the same dependency on large amounts of gas to function, there seems to be a more fundamental link between them, and this gave rise to models establishing the dependency of the star formation on the AGN properties through AGN feedback (Kauffmann & Haehnelt 2000; Hopkins et al. 2005; King 2005; Croton et al. 2006). Our results generally support such models in the sense that a significant fraction of X-ray AGN shows evidence of star formation. However, models requiring quenching of the star-formation activity as a result of AGN feedback (Hopkins et al. 2005) predict that at the latest stages, AGN residing in the red cloud are unobscured. This is not supported by our results, as there are no more obscured sources in the blue cloud (not shown in Fig. 3 for clarity purposes). Alternatively, the AGN could be enhancing the starburst activity instead of hindering it (King 2005), or AGN cooling could be regulated through a "radio mode"

(Croton et al. 2006) cutting the gas supply to the AGN. This could also explain radio emission coming from the AGN and the positions of such sources in the red cloud.

5.2. X-ray obscuration

In the models mentioned in the previous paragraph, star formation plays an important role in AGN evolution. Recent studies (e.g. Ballantyne et al. 2006) imply a connection between star formation and obscuration in X-rays and we can test this connection using radio emission as a probe of star formation activity.

Previous studies (Bauer et al. 2002; Georgakakis et al. 2004) have found a connection between those two properties, but we cannot confirm those results. We first consider whether selection effects could be responsible. Bauer et al. (2002) use the 1 Ms *Chandra* Deep Field North (CDF-N) survey which has detection limits very similar with the CDFS but they use a deeper radio survey, reaching depths of 40 μJy in 1.4 GHz, as opposed to our limit of 60 μJy. As a result their radio detection rate is higher and they report that a large fraction of the X-ray – radio matches lie close to the detection limit and would therefore be missed by our radio survey. They report that sources classified as "optically bright AGN" (having $-1 < \log\left(\frac{f_x}{f_{opt}}\right) < 1$ and optical magnitude $I < 24$) appear harder if radio detected. The statistical significance of this result is however poor, as the Gehan's test points out that the two hardness ratio distributions (for radio detected and non radio detected sources) are not different with a 83% probability. The small number of sources (13) in this analysis however limits the statistical results one can derive. In order to check if a larger sample would yield different results, we used all hard selected X-ray sources from the 3 arcmin sample of Bauer et al. (2002) and performed the classification used in this paper to select an AGN sample of 40 sources, 14 of which are radio identified. Performing the same test we find that the null hypothesis is 70% probable.

Georgakakis et al. (2004) on the other hand use similar radio limits (60 μJy at 1.4 GHz) with this study but have a shallower X-ray survey, their sources have $f_x(2-8\ \mathrm{keV}) > 7.7 \times 10^{-15}$ erg cm^{-2} s^{-1}. If we limit our sample to match the hard X-ray limits of Georgakakis et al. (2004) we again find no correlation; the Gehan's test gives a probability of 40% that the radio detected and non radio detected samples have from the same hydrogen column density distribution. This number refers to the E-CDFS case, where the sample is large enough (45 sources, 11 radio matches), so that small number statistics do not affect our results in great extent. Although our numbers are similar to Georgakakis et al. (2004, 43 sources, 14 radio matches), we cannot confirm their result.

The above result does not change if we limit our analysis to radio sources that are consistent with the radio-infrared correlation. Excluding sources with no infrared information from our sample and repeating the statistical tests results in a null hypothesis probability of 79%. The fact that we do not find any correlation between X-ray obscuration and radio emission means that the obscured and non obscured sources are not different in terms of their radio emission properties, and such an assumption is consistent with AGN unification models (e.g. Antonucci 1993). Indeed if we consider the standard scheme where absorption is attributed to a toroidal structure round the AGN and assume that this torus is connected with star formation (Wada & Norman 2002; Cid Fernandes et al. 2001), then only weak radio-obscuration correlation is expected because (starburst generated) radio emission is considered isotropic from the torus, whereas X-ray absorption is dependent on the line of sight. This setup explains the unobscured radio sources seen in Fig. 6. Our results therefore support AGN orientation-based unification models where the obscuring material is not symmetrically distributed, in contrast to models which favor spherical covering of the central engine (e.g. Fabian et al. 1998).

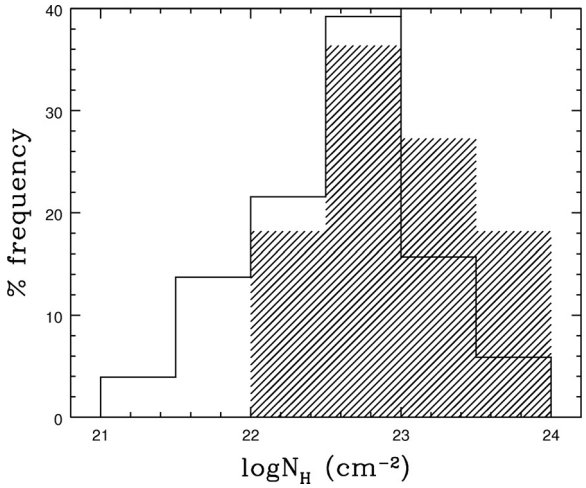

Fig. 7. Hydrogen column density (N_H) distributions for the subsample described in Sect. 5.2, i.e. hard X-ray selected radio quiet AGN which have an infrared counterpart and some degree of X-ray obscuration ($N_H > 10^{21}$ cm^{-2}). Shaded is the distribution for sources with a radio counterpart.

If this the case, the lack of correlation reflects the existence of sources hosting starburst activity, but the starburst clouds do not lie in the line of sight, thus being unobscured in X-rays. To check for this effect, we repeat the statistical test taking into consideration only sources with some degree of obscuration ($N_H > 10^{21}$ cm^{-2}). This sub-sample consists of 62 sources, 11 of which with a radio counterpart. The N_H histograms for sources in this sub-sample with and without a radio counterpart are shown in Fig. 7 and the statistical results show that there is a 97% probability that the populations of radio detected and non radio detected sources are *different* in terms of N_H. This supports the assumption that both the AGN contribution to the radio emission and the anisotropic distribution of the starburst (and radio emitting) clouds are responsible for the lack of correlation between radio emission and X-ray absorption.

6. Conclusions

We combine X-ray data of the southern *Chandra* Deep fields with radio observations of the same region. We aim to use the radio as a proxy of star formation activity and explore its relation to X-ray selected AGN. Optical and 24 μm infrared observations of the same region assist in defining the origin of the radio emission, as they offer independent means of tracing star formation. Our main results are summarized below:

- The radio detection rate of X-ray sources is 14% and 9% for the CDFS and the E-CDFS respectively, while 14% and 14% respectively of the hard selected sources have radio counterparts.
- There is evidence that the radio emission of up to 60% of the radio detected X-ray sources is linked to star formation. There is also a number of sources whose radio emission is attributed to the AGN; the radio-infrared correlation and the color distribution can identify them.

- As derived by the $L_{24\ \mu m} - L_{1.4\ GHz}$ relation, we do not find strong evidence for the presence of numerous radio excess AGN which are not detected in the 1 Ms CDFS exposure.
- We found no strong evidence of correlation between radio emission and X-ray absorption. This is partly a result of the AGN being responsible for the radio emission of some sources and partly a result of the obscuring material being anisotropically distributed.

Acknowledgements. E.R. acknowledges funding from the European Social Fund, Operational Program for Educational and Vocational Training II (EPEAEK II), and in particular the Program PYTHAGORAS II. A.G. acknowledges financial support from the Marie-Curie Fellowship grant MEIF-CT-2005-025108. J.A. gratefully acknowledges the support from the Science and Technology Foundation (FCT, Portugal) through the research grant POCI/CTE-AST/58027/2004.

References

Afonso, J., Georgakakis, A., Almeida, C., et al. 2005, ApJ, 624, 135
Afonso, J., Mobasher, B., Koekemoer, A., Norris, R. P., & Cram, L. 2006, AJ, 131, 1216
Alexander, D. M., Bauer, F. E., Brandt, W. N., et al. 2003, AJ, 126, 539
Antonucci, R. 1993, ARA&A, 31, 473
Appleton, P. N., Fadda, D. T., Marleau, F. R., et al. 2004, ApJS, 154, 147
Ballantyne, D. R., Everett, J. E., & Murray, N. 2006, ApJ, 639, 740
Barger, A. J., Cowie, L. L., Mushotzky, R. F., et al. 2005, AJ, 129, 578
Barger, A. J., Cowie, L. L., Wang, W.-H. 2007, ApJ, 654, 764
Bauer, F. E., Alexander, D. M., Brandt, W. N., et al. 2002, AJ, 124, 2351
Bauer, F. E., Alexander, D. M., Brandt, W. N., et al. 2004, AJ, 128, 2048
Bell, E. F., Wolf, C., Meisenheimer, K., et al. 2004, ApJ, 608, 752
Bressan, A., Silva, L., & Granato, G. L. 2002, A&A, 392, 377
Condon, J. J., Huang, Z.-P., Yin, Q. F., & Thuan, T. X. 1991, ApJ, 378, 65
Chapman, S. C., Barger, A. J., Cowie, L. L., et al. 2003, ApJ, 585, 57
Cid Fernandes, R., Heckman, T., Schmitt, H., González Delgado, R. M., & Storchi-Bergmann, T. 2001, ApJ, 558, 81
Croton, D., Springel, V., White, S. D. M., et al. 2006, MNRAS, 365, 11
Davis, M., Guhathakurta, P., Konidaris, N., et al. 2007, ApJL, in press [arXiv:astro-ph/0607355]
Donley, J. L., Rieke, G. H., Rigby, J. R., & Pérez-González, P. G. 2005, ApJ, 634, 169D
Fabian, A. C., Barcons, X., Almaini, O., & Iwasawa, K. 1998, MNRAS, 297, L11
Falcke, H., Nagar, N. M., Wilson, A. S., & Ulvestad, J. S. 2000, ApJ, 542, 197
Fanaroff, B. L., & Riley, J. M. 1974, MNRAS, 167, 31
Farrah, D., Afonso, J., Efstathiou, A., et al. 2003, MNRAS, 343, 585
Ferrarese, L., & Merritt, D. 2000, ApJ, 539, L9
Franceschini, A., Manners, J., Polletta, M., et al. 2005, AJ, 129, 2074
Gebhardt, K., Bender, R., Bower, G., et al. 2000, ApJ, 539, L13
Georgakakis, A., Mobasher, B., Cram, L., et al. 1999, MNRAS, 306, 708
Georgakakis, A., Hopkins, A. M., Afonso, J., et al. 2004, MNRAS, 354, 127
Hasinger, G., Miyaji, T., & Schmidt, M. 2005, A&A, 441, 417
Helou, G., Soifer, B. T., & Rowan-Robinson, M. 1985, ApJ, 298, L7
Hopkins, P. F., Hernquist, L., Cox, T. J., et al. 2005, ApJ, 630, 705
Isobe, T., Feigelson, E. D., & Nelson, P. I. 1986, ApJ, 306, 490
Kauffmann, G., & Haenhelt, M. 2000, MNRAS, 311, 576
Kauffmann, G., Heckman, T. M., Tremonti, C., et al. 2003, MNRAS, 346, 1055
Kellermann, K. I., Sramek, R., Schmidt, M., Shaffer, D. B., & Green, R. 1989, AJ, 98, 1195
King, A. 2005, ApJ, 635, L121
Lavalley, M., Isobe, T., & Feigelson, E. 1992, ASPC, 25, 245
Le Fèvre, O., Vettolani, G., Paltani, S., et al. 2004, A&A, 428, 1043
Lehmer, B. D., Brandt, W. N., Alexander, D. M., et al. 2005, ApJS, 161, 21
Lutz, D., Sturm, E., Genzel, R., Moorwood, A. F. M., & Sternberg, A. 1997, Ap&SS, 248, 217
Magorrian, J., Tremaine, S., Richstone, D., et al. 1998, AJ, 115, 2285
Mignoli, M., Cimatti, A., Zamorani, G., et al. 2005, A&A, 437, 883
Mushotzky, R. 2004, in Supermassive Black Holes in the Distant Universe, ed. A. J. Barger
Nagar, N. M., Falcke, H., Wilson, A. S., & Ulvestad, J. S. 2002, A&A, 392, 53
Nandra, K., & Pounds, K. A. 1994, MNRAS, 268, 405
Nandra, K., Georgakakis, A., Willmer, C. N. A., et al. 2007, ApJL, in press [arXiv:astro-ph/0607270]
Sanders, D. B., & Mirabel, I. F. 1996, ARA&A, 34, 749
Szokoly, G. P., Bergeron, J., Hasinger, G., et al. 2004, ApJS, 155, 271
Taylor, G. B., Vermeulen, R. C., Readhead, A. C. S., et al. 1996, ApJS, 107, 37
Vanzella, E., Cristiani, S., Dickinson, M., et al. 2005, A&A, 434, 53
Vanzella, E., Cristiani, S., Dickinson, M., et al. 2006, A&A, 454, 423
Wada, K., & Norman, C. A. 2002, ApJ, 566, L21
Willmer, C. N. A., Faber, S. M., Koo, D. C., et al. 2006, ApJ, 647, 853
Wolf, C., Meisenheimer, K., Kleinheinrich, M., et al. 2004, A&A, 421, 913
Wu, Hong, Cao, Chen, Hao, Cai-Na, et al. 2005, ApJ, 632, L79
Zheng, W., Mikles, V. J., Mainieri, V., et al. 2004, ApJS, 155, 73